Journal of Materials Chemistry A

Accepted Manuscript

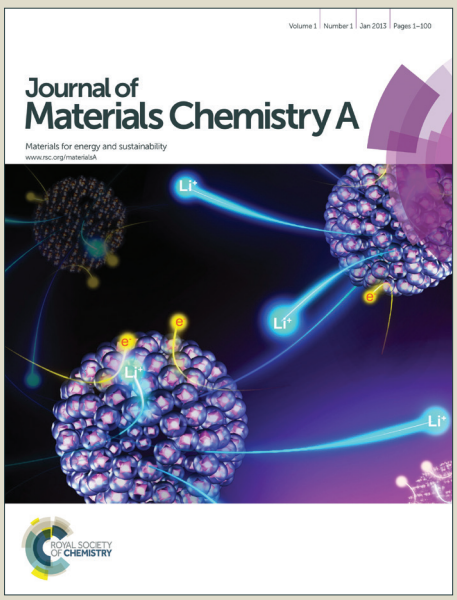

ROYAL SOCIETY OF CHEMISTRY

www.rsc.org/materialsA

Cite this: DOI: 10.1039/c0xx00000x

www.rsc.org/xxxxxx

ARTICLE TYPE

Lithium Amidoborane Hydrazinates: Synthesis, Structure and Hydrogen Storage Properties

Teng He,[a] Hui Wu[b,c], Guotao Wu*[a] , Zhao Li[a], Wei Zhou[b,c], Xiaohua Ju[a], Dong Xie[a], Ping Chen[a,d]

Received (in XXX, XXX) Xth XXXXXXXXX 20XX, Accepted Xth XXXXXXXXX 20XX

DOI: 10.1039/b000000x

The first metal amidoborane hydrazinate with the composition of $LiNH_2BH_3 \cdot NH_2NH_2$ was successfully synthesized and characterized in the present study. $LiNH_2BH_3 \cdot NH_2NH_2$ exhibits a monoclinic $P2_1/n$ space group with lattice parameters of a = 10.0650 Å, b = 6.3105 Å, c = 7.4850 Å, and β = 107.497º. Meanwhile, lithium amidoborane hydrazinates with different molar ratios of $LiNH_2BH_3$ (LiAB) and NH_2NH_2 were synthesized and characterized. It is found that 4LiAB-NH_2NH_2 can release 1.6 equiv. and 2.5 equiv. H_2/LiAB at 75 °C and 170 °C, respectively. Therefore, around 7.1 wt% and 11.1 wt% hydrogen can be released form 4LiAB-NH_2NH_2 at 75 °C and 170 °C, respectively, which are higher than those of pristine LiAB. The dehydrogenation mechanism, which may be initiated by the "homogeneous dissociation" of N-N in hydrazine, was also proposed and discussed in this study.

1. Introduction

Development of efficient hydrogen storage materials on board is one of the greatest challenges towards the realization of "hydrogen economy".[1, 2] In the past decade, tremendous effects have been given to ammonia borane (AB for short),[3, 4] which has a hydrogen content as high as 19.6 wt%. However, the high kinetic barrier, by-products, and sample foaming during dehydrogenation make AB unsuitable for application on PEMFC vehicle. To overcome these obstacles, researchers have investigated several approaches and improved the dehydrogenation properties by using nanoscaffolds,[5, 6] transition metal catalysts,[7, 8] acid or base catalysts,[9, 10] and ionic liquid[11]. Another important method is to replace one H atom on NH_3 in AB by alkali (Li,[12, 13] Na[14] and K[15]) or alkaline-earth metals(Mg[16], Ca[17, 18] and Sr[19]), forming metal amidoboranes. Due to the substitution of metal ions, the length of N-B bond is shortened, resulting in the activation of N-H bond and B-H bond in amidoboranes[12, 13]. As a consequence, the dehydrogenation temperature is reduced to a lower region, which is accompanied with the suppression of by-product borazine at the same time. In the following research, bimetal amidoboranes [20-22] are obtained as a result of milling LiH-NaH or NaH-MgH_2 mixtures with AB with favorable dehydrogenation properties. Chua *et al.* synthesized calcium amidoborane diammoniate ($CaAB \cdot 2NH_3$) and found that $CaAB \cdot 2NH_3$ can evolve ammonia at elevated temperatures forming calcium amidoborane (CaAB) in an open system. However, the ammonia ligands can interact with CaAB and trigger hydrogen release at 70°C if a close vessel was employed[23]. Similarly, lithium amidoborane ($LiNH_2BH_3$; LiAB in short) can also absorb/desorb ammonia reversibly at room temperature and form corresponding ammoniate ($LiAB \cdot NH_3$)[24] at low temperature. The decomposition of $LiAB \cdot NH_3$ releases 3.0 equiv H_2 (11.18 wt%) rapidly under ammonia. In addition, magnesium amidoborane triammoniate ($MgAB \cdot 3NH_3$)[25] can release hydrogen and ammonia in open system upon heating. Whereas, magnesium amidoborane monoammoniate ($MgAB \cdot NH_3$)[26] starts to release H_2 rather than NH_3 under dynamic flow, which is quite different from that of $CaAB \cdot 2NH_3$ and $MgAB \cdot 3NH_3$. Therefore, the ligand ammonia plays a very important role not only in the stabilization of amidoboranes, but also in the dehydrogenation. It was reported that the dehydrogenation mechanism of metal amidoboranes likely followed the combination of protonic $H^{\delta+}$ and hydridic $H^{\delta-}$ into hydrogen[12, 13]. However, there are unequal $H^{\delta+}$ and $H^{\delta-}$ in amidoboranes which could be balanced by the protonic $H^{\delta+}$ in the ligand NH_3. In the above mentioned ammoniates, the combination of $H^{\delta+}$ in NH_3 and $H^{\delta-}$ in BH_3 is one of the driving forces for dehydrogenation[27]. Thus, it is of great interest to probe other $H^{\delta+}$ containing ligands to balance the $H^{\delta+}$ and $H^{\delta-}$ in amidoborane and improve the dehydrogenation properties.

Recently, hydrazine (NH_2NH_2) with a hydrogen content of 12.5 wt% has received considerable attention. Singh *et al.* used bimetal catalysts to realize total conversion of hydrazine into hydrogen and nitrogen at room temperature.[28, 29] While, He *et al.* used a noble-metal-free catalysts to catalyze the decomposition of hydrazine hydrate and found 100% conversation and more than 93 % selectivity to hydrogen[30]. Hydrazine can also coordinate with borane to form $NH_2NH_2 \cdot BH_3$ and $NH_2NH_2 \cdot 2BH_3$.[31-33] To optimize the dehydrogenation properties of hydrazine borane, alkali metal hydrides were introduced to react with hydrazine and $NH_2NH_2 \cdot BH_3$ to synthesize metal hydrazide and metal hydrazinoborane, respectively.[34-37] Additionally, hydrazine can also be used for regenerating AB or LiAB in liquid ammonia solution,[38-40] where the yield of AB was claimed as high as 95%. It is worth mentioning that, according to the concept of

combination of $H^{\delta+}$-$H^{\delta-}$, hydrazine was employed as a ligand and hence complexed with borohydrides to form hydrazinates in our recent results.[41, 42] As a ligand, hydrazine exhibited great improvement in the dehydrogenation of borohydrides. Therefore, it is suggested that hydrazine should be considered as a ligand in amidoboranes. As there are four $H^{\delta+}$s in one hydrazine molecule, the unequal $H^{\delta+}$ and $H^{\delta-}$ in amidoborane could be modified, which may consequently improve the dehydrogenation performance. In addition, from chemical point of view, hydrazine can coordinate with metal in amidoboranes and form a serial of new compounds, which would exhibit many crystallographically interesting structures. Therefore, the first example of amidoborane hydrazinate is synthesized, characterized and investigated in the present work. Experimental results show that $LiNH_2BH_3{\cdot}NH_2NH_2$ exhibits a monoclinic structure with a $P2_1/n$ space group and lattice parameters of a = 10.0650 Å, b = 6.3105 Å, c = 7.4850 Å, and β = 107.497º. Particularly, a composition of 4LiAB-NH_2NH_2 can release 7.1 wt% and 11.1 wt% hydrogen at 75 °C and 170 °C, respectively, which are higher than those of pristine LiAB.

2. Experimental

2.1 Materials synthesis

LiH (Sigma, 97.0%) $NaBH_4$ (Aldrich, 98.0%) $(NH_4)_2CO_3$ (Alfa, 99%) were used without further purification. AB was synthesized from the reaction of $NaBH_4$ and $(NH_4)_2CO_3$ in THF solution. LiAB was synthesized according to the reaction between LiH and AB ($LiH + NH_3BH_3 \rightarrow LiNH_2BH_3 + H_2$) in literature [12]. To synthesize lithium amidoborane hydrazinates, around 200 mg self-made LiAB and calculated stoichiometric amount of hydrazine were placed separately in a sealed bottle at room temperature. Due to the vapor pressure of hydrazine, hydrazine can automatically absorb into amidoborane overnight. The samples were then ball milled on a Retsch PM 400 planetary mill at 100 rpm under an inert atmosphere for 2 h.[42] After synthesis, the qualities of AB, LiAB and nLiAB-NH_2NH_2 were examined by X-ray diffraction (XRD).

Regeneration of spent fuel of nLiAB-NH_2NH_2 was carried out in liquid NH_3 solution. Around 100 mg dehydrogenated products of nLiAB-NH_2NH_2 and 400 mg hydrazine were suspended in liquid ammonia at 0 °C in a close vessel. Then, the reactor was heated to 40 °C and kept for 3 days with continuous stirring. Ammonia and hydrazine were removed at room temperature under vacuum for 3 hours. At last, the solid product was dissolved in THF for ^{11}B nuclear magnetic resonance (NMR) examination.

2.2 Characterizations

A home-made temperature programmed desorption-mass spectroscopy (TPD-MS) combined system was employed to detect the gaseous product during sample decomposition. XRD characterizations were conducted on a PANalytical X'pert diffractometer (Cu Kα, 40 kV, 40 mA) To avoid air contamination, samples were sealed in a home-made sample holder covered by a piece of shielding film. The high-resolution XRD data were collected from diffractometer at BL14B1 beamline of Shanghai Synchrotron Radiation Facility (λ=1.239800 Å). During the measurements, the sample was sealed in a capillary with a diameter of 0.5 mm. Volumetric release measurements were performed on a home-made Sievert type apparatus to quantify the gas evolution.

Liquid ^{11}B NMR and solid state ^{11}B magic angle spinning nuclear magnetic resonance (MAS NMR) experiments were carried out at room temperature on Bruker AVANCE 500MHz (11.7 T) spectrometer at a frequency of 128.3 MHz. The chemical shifts of liquid and solid NMR for ^{11}B nucleiare referenced to BF_3 at 0 ppm and $LiBH_4$ at 41 ppm, respectively.

Ammonia concentration in the gaseous products was determined by using a Thermo conductivity meter，while the accumulated gaseous product was bubbled into a dilute H_2SO_4 solution and the change in ion conductivity of the solution was monitored.

2.3 First-principles calculations method

First-principles calculations were performed using the plane-wave implementation of density functional theory (DFT) in the PWscf package. The Vanderbilt-type ultrasoft potential and the generalized gradient approximation (GGA) of Perdew-Burke-Ernzerh for the exchange-correlation energy functional were used. A cutoff energy of 408 eV was found to be enough for the total energy and force to converge within 0.5 meV/atom and 0.005 eV/Å. Car-Parrinello molecular dynamics simulation was used to help searching for the most likely crystal structures. The conventional unit cell was used with cell dimensions fixed at the experimental values. The initial system temperature was set to 600 K. The system was first allowed to evolve and equilibrate for 20 ps, and then the system temperature was slowly brought to 0 K in a period of 20 ps. Structure optimizations on the resulting candidate structures at 0 K were further performed with respect to atomic positions with the lattice parameters fixed at the experimental values. Lattice dynamics calculations were then performed on the relaxed structures to rule out unstable candidates. The total energies of the stable candidate structures at 0 K, including corrections for the zero-point motion, were also evaluated. This information was used in combination with XRD pattern matching to derive the best crystal structure solutions of the LiAB hydrazinate.

3. Results and Discussion

3.1 Formation of $nLiNH_2BH_3$-NH_2NH_2 and crystal structure of $LiNH_2BH_3{\cdot}NH_2NH_2$

The reactions of LiAB with hydrazine in molar ratios of 1:1 and 2:1 yield two new phases as identified by XRD technique (shown in Figure S1). However, a slurry state mixture could be obtained by adding more hydrazine to LiAB (for example 1:2 in molar ratio). And, reducing hydrazine content to the molar ratio of 4:1 (LiAB:hydrazine) will result in mixed phases of 2LiAB-NH_2NH_2 and LiAB (Figure S1). The XRD pattern of $LiAB{\cdot}NH_2NH_2$ was indexed using a monoclinic $P2_1/n$ space group with lattice parameters of approximately a = 10.0650 Å, b = 6.3105 Å, c = 7.4850 Å, and β = 107.497º. The crystal structure was then partially solved using direct space methods under this space group. Due to the uncertain H positions, first-principles molecular dynamics simulated annealing were then performed to confirm the LiAB and NH_2NH_2 configuration with the lowest energy. Rietveld structural refinement on the optimal structural candidate

was performed using the GSAS package on the XRD data. The LiAB and NH_2NH_2 were kept as rigid bodies with common refined bond lengths and bond angles constrained as reasonable values due to the inadequate number of observations. One LiAB and one NH_2NH_2 group together with lattice parameters were refined, yielding the agreement factors of R_{wp} = 0.0222, R_p = 0.0172 and χ^2 = 1.693. The Rietveld fit to the XRD pattern is shown in Figure 1.

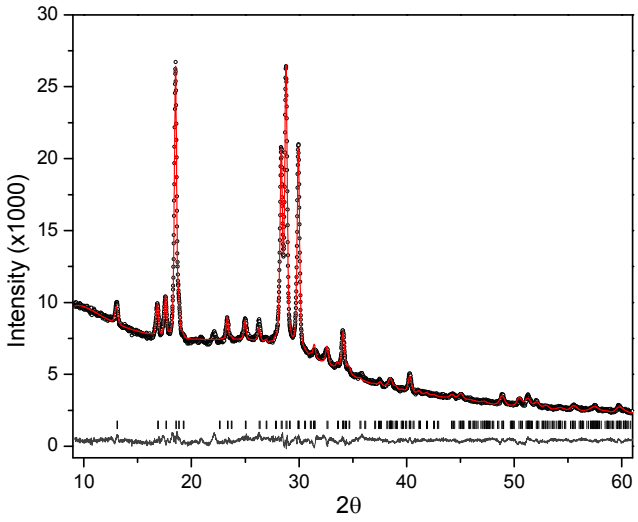

Fig. 1 Experimental (circles), fitted (line), and difference (line below observed and calculated patterns) XRD profiles for LiAB·NH_2NH_2 at 298 K (CuKa radiation). Vertical bars indicate the calculated positions of Bragg peaks.

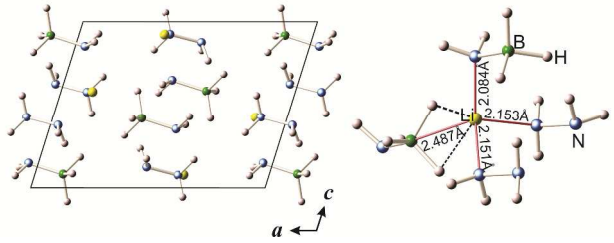

Fig. 2 Crystal structure of LiAB·NH_2NH_2 (left) and local coordination (right) of Li^+ cation.

Table 1 Interatomic distances (Å) in LiAB·NH_2NH_2 compared with pristine LiAB and hydrazine at room temperature.

	LiAB·NH_2NH_2	LiAB[13]	NH_2NH_2[43]
Li-N	2.084 (Li-NH_2BH_3) 2.151-2.153 (Li-NH_2NH_2)	2.063	-
N-H	1.027 (LiAB) 1.027-1.031 (NH_2NH_2)	1.025-1.026	1.021
B-H	1.238-1.255	1.236-1.248	-
N-N	1.455	-	1.449
B-N	1.548	1.547	-

The crystal structure of LiAB·NH_2NH_2 and local coordination of Li^+ cation are shown in Figure 2 , and the interatomic distances in LiAB·NH_2NH_2 as compared with pristine LiAB and pristine hydrazine can be found in Table 1. In LiAB·NH_2NH_2, each Li^+ cation is surrounded by two $NH_2BH_3^-$ ions and two NH_2NH_2 molecules, leading to a distorted tetrahedral coordination. The distances between Li^+ and N in the adjacent NH_2NH_2 are 2.151 Å and 2.153 Å, similar to the Li-N distances in other coordinate bonds, such as $LiBH_4$·NH_2NH_2 (2.131-2.427 Å).[41] At the same time, the Li^+ directly bonds with a $NH_2BH_3^-$ ions with the closest Li-N distance of 2.084 Å, similar to Li-N distances in ionic bonds, such as LiAB (2.063 Å) and $LiNH_2$ (2.06-2.21 Å)[13]. In addition, each Li^+ is also coordinated with the other $NH_2BH_3^-$ group with a Li-B distance of 2.487 Å. Therefore, the coordination of Li^+ is consistent with the Li (IV) tetrahedral coordination preferred in the commonly observed complex hydrides, *e.g.*, $LiNH_2$, $LiBH_4$[44] and LiAB.[13] Unfortunately, the crystal structure of 2LiAB-NH_2NH_2 is still unresolved due to the poor quality of XRD pattern.

Since the coordination of NH_2NH_2 to LiAB is through the donation of a lone pair electrons, Li^+ will bear higher electron density than Li^+ in pristine LiAB, resulting in the elongated Li-N distance (Li-NH_2BH_3) in LiAB·NH_2NH_2 as shown in Table 1. Similarly, due to the lower electrons density of N, N-H (in NH_2NH_2 ligand) distances in LiAB·NH_2NH_2 are longer than that of the pristine hydrazine. In addition, two N atoms in hydrazine are coordinated by two Li^+, the distance between N-N is elongated consequently, showing the activation of ligand hydrazine compared with the pristine one. Moreover, the B-H distance and N-H (in LiAB) in LiAB·NH_2NH_2 are longer than those of the pristine LiAB, indicating the activation of N-H and B-H bonds after coordinating with hydrazine. From the crystal structure, it was found that the $H^{\delta+}$ (in NH_2NH_2 or NH_2BH_3) has a short distance with its neighboring $H^{\delta-}$ in BH_3, ranging from 1.888 to 2.139 Å, which indicates the establishment of dihydrogen bonding network. Such interaction of the oppositely charged $H^{\delta+}$ (in NH_2NH_2 and NH_2) and $H^{\delta-}$ (in BH_3^-) may consequently also contribute to the elongated N-H and B-H bonds in LiAB·NH_2NH_2 . It is reported that the dihydrogen bonding network in ammonia borane[3, 45] is primarily responsible for the stability of the molecular crystal at room temperature. The dihydrogen bonding network and the ionic/electrostatic interactions between Li and NH_2BH_3/N_2H_4 ligands in LiAB·NH_2NH_2 are thus responsible for the structural stabilization and is expected to have a profound impact on their thermal decomposition.

3.2 Decomposition and dehydrogenation of nLiNH_2BH_3-NH_2NH_2

TPD-MS measurements are employed to investigate the dehydrogenation properties of nLiAB-NH_2NH_2 compared with the pristine LiAB as shown in Figure 3. Pristine LiAB releases hydrogen in two steps, giving a sharp peak centered at 92 °C and a broad peak centered at around 120 °C in the first and second step, respectively, which is identical to that in literature.[12] For LiAB·NH_2NH_2 sample (Figure 3b), it starts to release hydrogen at around 70 °C and exhibits three successive steps. However, a large amount of ammonia, which is a poison to fuel cells, is also observed during dehydrogenation. The evolution of NH_3 should be attributed to the excess of N in the system. Therefore, to suppress ammonia evolution, the content of hydrazine was reduced to 2:1 (LiAB:NH_2NH_2) in a molar ratio (Figure 3c). It can be seen that the dehydrogenation of 2LiAB-NH_2NH_2 is a two-steps reaction with the peak temperatures centered at 74 °C and 130 °C. As we expected, only a little amount of ammonia can be detected. If we further decrease the ratio of NH_2NH_2 /LiAB to

4:1 (*i.e.*, 4LiAB-NH_2NH_2 in Figure 3d), which possesses equal amount of $H^{\delta+}$ and $H^{\delta-}$, no ammonia can be detected from MS. At the same time, the dehydrogenation profile of 4LiAB-NH_2NH_2 is similar to that of 2LiAB-NH_2NH_2 with dehydrogenation peak temperatures at 76 °C and 130 °C. It is noticeable that the dehydrogenation temperature of the first step of 2LiAB-NH_2NH_2 and 4LiAB-NH_2NH_2 are about 17 °C lower than that of pristine LiAB, whereas, the second dehydrogenation temperatures are about 10 °C higher than that of pristine LiAB. It is reported that the decomposition of hydrazine follows two competitive routes giving rise to H_2 and N_2 or N_2 and NH_3 under mild conditions even with the presence of noble or noble metal-like catalysts[46-48]. However, no N_2 can be observed during the dehydrogenation/decomposition of nLiAB-NH_2NH_2. Therefore, the evolution of NH_3 during the decomposition of LiAB·NH_2NH_2 is not from the self-decomposition of hydrazine, which means the hydrogen is derived from the interaction of LiAB and hydrazine.

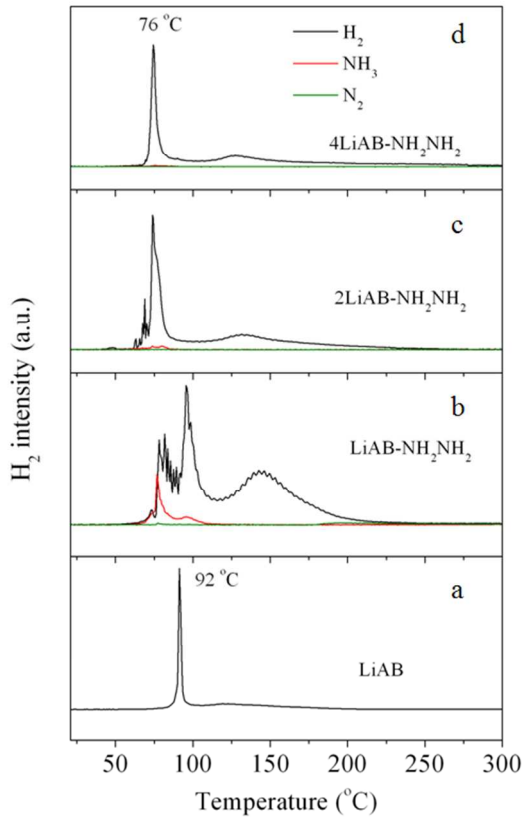

Fig. 3 TPD-MS results of nLiAB-NH_2NH_2 compared with pristine LiAB. (a: LiAB, b: LiAB-NH_2NH_2, c: 2LiAB-NH_2NH_2; d: 4LiAB-NH_2NH_2)

To quantify the evolution of hydrogen from nLiAB-NH_2NH_2 systems, volumetric release measurements were employed at 75 °C and 170 °C (Figure 4). At 75 °C, around 1.2 equiv. H_2/LiAB can be released from the pristine LiAB in 3 hours. However, LiAB·NH_2NH_2 system can release around 1.5 equiv. gas/LiAB, which is composed of NH_3 and H_2 determined by MS. For 2LiAB-NH_2NH_2 and 4LiAB-NH_2NH_2 systems, around 1.6 equiv. H_2/LiAB are generated from both samples under the same condition. At the same time, we can see that the onset dehydrogenation temperatures of 2LiAB-NH_2NH_2 and 4LiAB-NH_2NH_2 are lower than that of the pristine LiAB, which is consistent with TPD results. It is worth mentioning that, calculating from the volumetric release measurements, around 7.1 wt% hydrogen can be evolved from 4LiAB-NH_2NH_2 component at 75 °C, which is higher than that of the pristine LiAB (6.5 wt%). At 75 °C, around 14.1 mol% ammonia is found in the gaseous products of LiAB·NH_2NH_2, agreeing with the TPD result. However, the concentration of by-product ammonia is even lower than 0.2 mol% in the 2LiAB-NH_2NH_2 and 4LiAB-NH_2NH_2 samples as shown in Table S1.

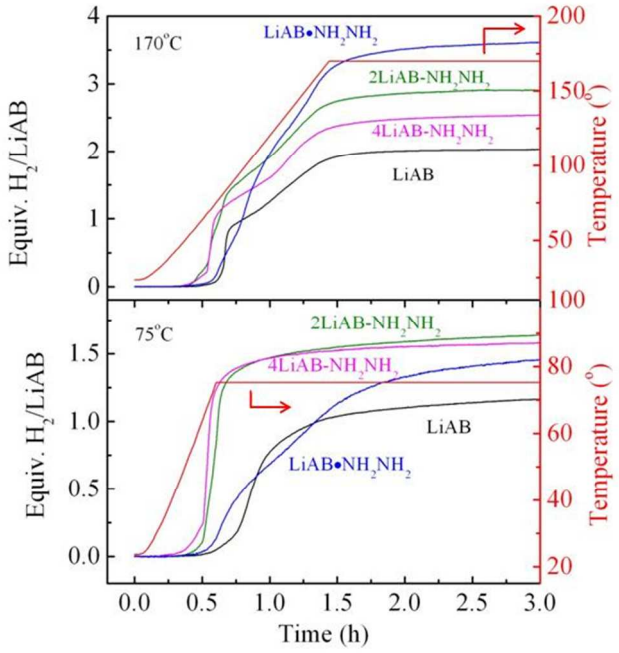

Fig. 4 Volumetric release measurements on LiAB complexed with hydrazine with different molar ratios compared with pristine LiAB at 75 °C and 170 °C

For the pristine LiAB, around 2 equiv. H_2 can be released at 170 °C, identical to the literatures.[12, 13] Under the same condition, LiAB·NH_2NH_2 can release more than 3.6 equiv. gas, which is composed of hydrogen and ammonia as detected by MS. However, around 2.9 and 2.5 equiv. H_2/LiAB can be released from 2LiAB-NH_2NH_2 and 4LiAB-NH_2NH_2. In other words, around 10.9 wt% and 11.1 wt% hydrogen can be evolved from these two samples at 170 °C. The weight loss of 4LiAB-NH_2NH_2 from TG experiment (Figure S2) is about 11.2 wt% at 200 °C which is consistent with the volumetric release result, indicating the high purity of hydrogen production. However, the weight loss is about 18.7 wt% for 2LiAB-NH_2NH_2 at 200 °C (Figure S3), which is much higher than the value of 10.9 wt% from volumetric release measurement, indicating the gaseous impurity (NH_3) release during TG experiment. The low impurity (NH_3) concentration may be attributed to the fact that the formed ammonia has more chance to interact with LiAB or solid products during the volumetric release measurement[41, 49]. However, in the TG measurement, ammonia will be taken away by the carrier gas once formed. Therefore, the weight loss form TG is much higher than that from the volumetric release measurement. The exothermic nature of dehydrogenation of 2LiAB-NH_2NH_2 and 4LiAB-NH_2NH_2 from DTA (Figure S2 and S3) indicates the

irreversibility of the dehydrogenation process. The following investigation focuses on 2LiAB-NH_2NH_2 and 4LiAB-NH_2NH_2 samples due to the low ammonia concentration in the gaseous products. XRD was also employed to characterize the solid products after dehydrogenation at 75 °C and 170 °C. However, all the dehydrogenated products are in an amorphous state. According to the quantity of hydrogen evolution, the dehydrogenation reactions can be expressed as follow:

$$2LiNH_2BH_3 \cdot NH_2NH_2 \xrightarrow{170^oC} 2[LiN_2BH] + 6H_2 \quad R1$$

$$4LiNH_2BH_3 \cdot NH_2NH_2 \xrightarrow{170^oC} 2[Li_2N_3B_2H_2] + 10H_2 \quad R2$$

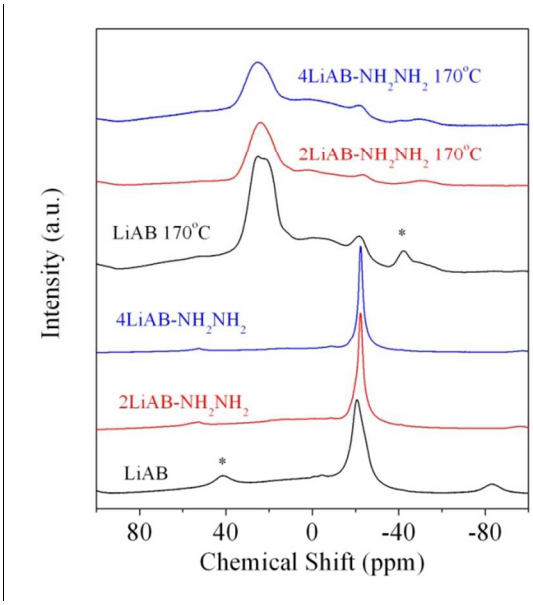

Fig. 5 ^{11}B MAS NMR spectra of synthesized nLiAB-NH_2NH_2 and post dehydrogenated nLiAB-NH_2NH_2 at 170 °C compared with pristine LiAB.

Since the dehydrogenated products are of amorphous state, ^{11}B MAS NMR technique was carried out to investigate the chemical environment of the post-dehydrogenated products. As shown in Figure 5, the pristine LiAB exhibits a peak at around -21.6 ppm which belongs to BH_3 signal.[12] Both synthesized 2LiAB-NH_2NH_2 and 4LiAB-NH_2NH_2 samples show BH_3 signals at around -22.3 ppm, indicating the formation of new phases. From XRD results (Figure S1), the 4LiAB-NH_2NH_2 sample is composed of LiAB and 2LiAB-NH_2NH_2 phases. However, there is only one peak in 4LiAB-NH_2NH_2 at around -22.3 ppm. No signal or shoulder peak at around -21.6 ppm for pristine LiAB can be observed. This may be attributed to the overlap of LiAB and 2LiAB-NH_2NH_2 signals in the solid NMR measurement. It is worth noting that the chemical shift of ^{11}B in 2LiAB-NH_2NH_2 has 0.7 ppm up-shift compared to the pristine LiAB, which is consistent with that of CaAB·$2NH_3$ in the literature.[23] The post decomposed LiAB sample at 170 °C gives a broad peak ranging from 33 ppm to 15 ppm, which is consistent with the amorphous [LiNBH] reported in the literatures[12, 13]. For the 2LiAB-NH_2NH_2 and 4LiAB-NH_2NH_2 samples, there is still a little amount of BH_3 residue after dehydrogenation at 170 °C as shown in Figure 5. Most of the ^{11}B signal in the products are sp^2 hybridized B species, maybe in the form of Li_3BN_2, [BN_2H] or [BN_3], which is similar to the decomposition of ammonia borane family[50-52].

Due to the exothermic nature of dehydrogenation (Figure S2 & S3), it is unlikely to achieve the direct hydrogenation from the spent fuel of nLiAB-NH_2NH_2. However, it is reported that AB or LiAB can be regenerated by interaction of the spent fuel with hydrazine in NH_3 solution[38-40]. Therefore, we investigated the regeneration of spent fuel of 4LiAB-NH_2NH_2 by using hydrazine in NH_3 solution at 40 °C. From liquid NMR technique (Figure S4), two BH_3 species can be observed after regeneration, which can be assigned to $BH_3NH_2NH_2$ and NH_3BH_3. Therefore, the regeneration of BH_3 species can be realized. However, LiAB and nLiAB-NH_2NH_2 compounds are not observed. It is worth mentioning that the yield of regenerated BH_3 species is less than 10% and possible for further optimization.

3.3 Discussion on the dehydrogenation pathway

Due to the unbalanced $H^{\delta+}$ and $H^{\delta-}$ in LiAB, hydrazine with four $H^{\delta+}$ in one molecule was selected and complexed with LiAB. It is known that the decomposition of hydrazine follows two competitive ways (R3 and R4)[46-48]:

$$NH_2NH_2 \longrightarrow N_2 + 2H_2 \quad R3$$

$$3NH_2NH_2 \longrightarrow N_2 + 4NH_3 \quad R4$$

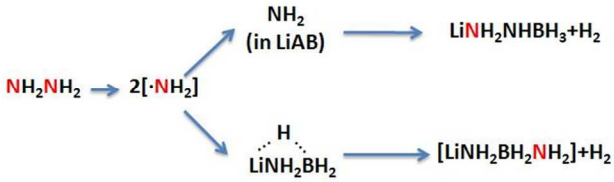

Scheme 1 Proposed dehydrogenation pathways of 2$LiNH_2BH_3$-NH_2NH_2

Since nitrogen was not observed during the decomposition of *n*LiAB-NH_2NH_2, hydrogen is not from the self-decomposition of hydrazine. As mentioned above, the elongated B-H and N-H bonds in LiAB·NH_2NH_2 showed the activation of both hydrazine and LiAB. Consequently, we propose that the hydrogen release is more likely *via* the interaction of LiAB and NH_2NH_2. Here, two dehydrogenation pathways of 2LiAB-NH_2NH_2 are proposed as illustrated in Scheme 1. Since the dissociation energy of N-N bond (60 kJ mol^{-1}) is lower than that of N-H bond (84 kJ mol^{-1}) in hydrazine[53, 54], the "homogeneous dissociation" of N-N bond forming [$\cdot NH_2$] radicals may occur, which is observed in the surface of metal catalysts[46]. The radical [$\cdot NH_2$] is an active species and can react with LiAB readily. Therefore, [$\cdot NH_2$] may attack NH_2 group in $LiNH_2BH_3$ forming lithium hydrazinoborane ($LiNH_2NHBH_3$)[34, 36] and H_2. It is reported that the lithium hydrazinoborane can be dehydrogenated readily under mild condition. For the second dehydrogenation pathway, it is reported that the bridged H between Li and B (Li···H···B) can be formed during the activation of LiAB[55-57], which is called "hydride transfer mechanism". The radical [$\cdot NH_2$] may attack the bridged H in BH_3 group forming [$LiNH_2BH_2NH_2$] and H_2, which may further decompose and release hydrogen in the following steps. For the LiAB·NH_2NH_2 sample, since more radical [$\cdot NH_2$] could be generated, the H atom generated from the interaction between [$\cdot NH_2$] and LiAB may have more chance to combine with excessive radical [$\cdot NH_2$] forming NH_3, which may in turn explain

the formation of large amount of NH_3 in TPD result of $LiAB{\cdot}NH_2NH_2$. For the $4LiAB\text{-}NH_2NH_2$ sample, two phases (LiAB and $2LiAB\text{-}NH_2NH_2$) can be observed from XRD. The decomposition of $2LiAB\text{-}NH_2NH_2$ is prior to that of pristine LiAB as shown in Figure 3. Therefore, LiAB may interact with the intermediate species of the decomposition of $2LiAB\text{-}NH_2NH_2$, forming $[Li_2N_3B_2H_2]$ and H_2 as shown in *R2*.

4. Conclusions:

The coordination of hydrazine to the Li^+ cation in lithium amidoborane results in the formation of hydrazinates, among which $LiNH_2BH_3{\cdot}NH_2NH_2$ is identified to crystallize in the monoclinic $P2_1/n$ space group. Around 7.1wt% hydrogen can be evolved from $4LiAB\text{-}NH_2NH_2$ component at 75 °C, which is higher than that of the pristine LiAB. Two possible dehydrogenation pathways for the hydrazinates are proposed. However, more investigations and characherizations are needed to obtain various metal amidoborane hydrazinates with appropriate dehydrogenation properties. Research effort shall also be devoted on the regenaration of amidoborane hydraiznates to realise the "reversibility" of these materials.

Acknowledgements

The authors would like to acknowledge financial support from the project of National Natural Science Funds for Distinguished Young Scholar (51225206), projects of National Natural Science Foundation of China (Grant Nos. U1232120, 51301161, 21473181 and 51472237) and project from Natural Science Fund of Liaoning Province, and Shanghai Synchrotron Radiation Facility (SSRF) for providing the beam time.

.

Notes and references

[a] *Dalian Institute of Chemical Physics, Chinese Academy of Sciences, 457, Zhongshan Road, Dalian, 116023, China. Fax:+86-411-84379583; Tel+86-411-84379583; E-mail: wgt@dicp.ac.cn*
[b] *NIST Center for Neutron Research, National Institute of Standards and Technology, Gaithersburg, Maryland, 20899-6102, USA*
[c] *Department of Materials Science and Engineering, University of Maryland College Park, Maryland, 20742-2115, USA*
[d] *State Key Laboratory of Catalysis, Dalian Institute of Chemical Physics, Chinese Academy of Sciences, 457, Zhongshan Road, Dalian, 116023, China*

† Electronic Supplementary Information (ESI) available: The supplementary crystallographic data of $LiNH_2BH_3{\cdot}NH_2NH_2$ was deposited in ICSD database, CSD number is 429145. XRD, TG-DTA, ^{11}B NMR. See DOI: 10.1039/b000000x/

1. http://www1.eere.energy.gov/hydrogenandfuelcells/storage/.
2. L. Schlapbach and A. Züttel, *Nature*, 2001, **414**, 353-358.
3. A. Staubitz, A. P. M. Robertson and I. Manners, *Chem. Rev.*, 2010, **110**, 4079-4124.
4. C. W. Hamilton, R. T. Baker, A. Staubitz and I. Manners, *Chem. Soc. Rev.*, 2009, **38**, 279-293.
5. A. Gutowska, L. Li, Y. Shin, C. M. Wang, X. Li, S. , J. Linehan, C. , R. S. Smith, B. Kay, D. , B. Schmid, W. Shaw, M. Gutowski and T. Autrey, *Angew. Chem. Int. Ed.*, 2005, **44**, 3578-3582.
6. Z. Tang, X. Chen, H. Chen, L. Wu and X. Yu, *Angew. Chem. Int. Ed.*, 2013, **52**, 5832-5835.
7. T. He, Z. Xiong, G. Wu, H. Chu, C. Wu, T. Zhang and P. Chen, *Chem. Mater.*, 2009, **21**, 2315-2318.
8. M. C. Denney, V. Pons, T. J. Hebden, D. M. Heinekey and K. I. Goldberg, *J. Am. Chem. Soc.*, 2006, **128**, 12048-12049.
9. D. W. Himmelberger, C. W. Yoon, M. E. Bluhm, P. J. Carroll and L. G. Sneddon, *J. Am. Chem. Soc.*, 2009, **131**, 14101-14110.
10. F. H. Stephens, R. T. Baker, M. H. Matus, D. J. Grant and D. A. Dixon, *Angew. Chem. Int. Ed.*, 2007, **46**, 746-749.
11. M. E. Bluhm, M. G. Bradley, R. Butterick, U. Kusari and L. G. Sneddon, *J. Am. Chem. Soc.*, 2006, **128**, 7748-7749.
12. Z. Xiong, C. K. Yong, G. Wu, P. Chen, W. Shaw, A. Karkamkar, T. Autrey, M. O. Jones, S. R. Johnson, P. P. Edwards and W. I. F. David, *Nat. Mater.*, 2008, **7**, 138-141.
13. H. Wu, W. Zhou and T. Yildirim, *J. Am. Chem. Soc.*, 2008, **130**, 14834-14839.
14. Z. Xiong, G. Wu, Y. S. Chua, J. Hu, T. He, W. Xu and P. Chen, *Energy Environ. Sci.*, 2008, **1**, 360-363.
15. H. V. K. Diyabalanage, T. Nakagawa, R. P. Shrestha, T. A. Semelsberger, B. L. Davis, B. L. Scott, A. K. Burrell, W. I. F. David, K. R. Ryan, M. O. Jones and P. P. Edwards, *J. Am. Chem. Soc.*, 2010, **132**, 11836-11837.
16. J. Luo, X. Kang and P. Wang, *Energy Environ. Sci.*, 2013, **6**, 1018-1025.
17. H. V. K. Diyabalanage, R. P. Shrestha, T. A. Semelsberger, B. L. Scott, M. E. Bowden, B. L. Davis and A. K. Burrell, *Angew. Chem. Int. Ed.*, 2007, **46**, 8995-8997.
18. J. Spielmann, G. Jansen, H. Bandmann and S. Harder, *Angew. Chem. Int. Ed.*, 2008, **120**, 6386-6391.
19. Q. A. Zhang, C. X. Tang, C. H. Fang, F. Fang, D. Sun, L. Z. Ouyang and M. Zhu, *J. Phys. Chem. C*, 2010, **114**, 1709-1714.
20. K. J. Fijalkowski, R. V. Genova, Y. Filinchuk, A. Budzianowski, M. Derzsi, T. Jaron, P. J. Leszczynski and W. Grochala, *Dalton Trans.*, 2011, **40**, 4407-4413.
21. H. Wu, W. Zhou, F. E. Pinkerton, M. S. Meyer, Q. Yao, S. Gadipelli, T. J. Udovic, T. Yildirim and J. J. Rush, *Chem. Commun.*, 2011, **47**, 4102-4104.
22. X. Kang, J. Luo, Q. Zhang and P. Wang, *Dalton Trans.*, 2011, **40**, 3799-3801.
23. Y. S. Chua, G. Wu, Z. Xiong, T. He and P. Chen, *Chem. Mater.*, 2009, **21**, 4899-4904.
24. G. Xia, X. Yu, Y. Guo, Z. Wu, C. Yang, H. Liu and S. Dou, *Chem. Eur. J.*, 2010, **16**, 3763-3769.
25. X. Kang, H. Wu, J. Luo, W. Zhou and P. Wang, *J. Mater. Chem.*, 2012, **22**, 13174-13179.
26. Y. S. Chua, G. Wu, Z. Xiong, A. Karkamkar, J. Guo, M. Jian, M. W. Wong, T. Autrey and P. Chen, *Chem. Commun.*, 2010, **46**, 5752-5754.
27. Y. S. Chua, W. Li, W. J. Shaw, G. Wu, T. Autrey, Z. Xiong, M. W. Wong and P. Chen, *ChemSusChem*, 2012, **5**, 927-931.
28. S. K. Singh and Q. Xu, *J. Am. Chem. Soc.*, 2009, **131**, 18032-18033.
29. S. K. Singh, X. B. Zhang and Q. Xu, *J. Am. Chem. Soc.*, 2009, **131**, 9894-9895.
30. L. He, Y. Huang, A. Wang, X. Wang, X. Chen, J. J. Delgado and T. Zhang, *Angew. Chem.*, 2012, **124**, 6295-6298.
31. T. Hügle, M. F. Kühnel and D. Lentz, *J. Am. Chem. Soc.*, 2009, **131**, 7444-7446.
32. R. Moury, G. Moussa, U. B. Demirci, J. Hannauer, S. Bernard, E. Petit, A. van der Lee and P. Miele, *Phys. Chem. Chem. Phys.*, 2012, **14**, 1768-1777.
33. L. Li, Y. Tan, Z. Tang, G. Xia, F. Yuan, Q. Li and X. Yu, *Mater. Chem. Phys.*, 2014, **143**, 1055-1060.
34. H. Wu, W. Zhou, F. E. Pinkerton, T. J. Udovic, T. Yildirim and J. J. Rush, *Energy Environ. Sci.*, 2012, **5**, 7531-7535.
35. R. Moury, U. B. Demirci, T. Ichikawa, Y. Filinchuk, R. Chiriac, A. van der Lee and P. Miele, *ChemSusChem*, 2013, **6**, 667-673.
36. R. Moury, U. B. Demirci, V. Ban, Y. Filinchuk, T. Ichikawa, L. Zeng, K. Goshome and P. Miele, *Chem. Mater.*, 2014, **26**, 3249-3255.
37. Y. S. Chua, Q. Pei, X. Ju, W. Zhou, T. J. Udovic, G. Wu, Z. Xiong, P. Chen and H. Wu, *J. Phys. Chem. C*, 2014, **118**, 11244-11251.
38. A. D. Sutton, A. K. Burrell, D. A. Dixon, E. B. Garner, J. C. Gordon, T. Nakagawa, K. C. Ott, P. Robinson and M. Vasiliu, *Science*, 2011, **331**, 1426-1429.
39. Z. Tang, H. Chen, X. Chen, L. Wu and X. Yu, *J. Am. Chem. Soc.*, 2012, **134**, 5464-5467.

40. Z. Tang, Y. Tan, X. Chen and X. Yu, *Chem. Commun.*, 2012, **48**, 9296-9298.
41. T. He, H. Wu, G. Wu, J. Wang, W. Zhou, Z. Xiong, J. Chen, T. Zhang and P. Chen, *Energy Environ. Sci.*, 2012, **5**, 5686-5689.
42. T. He, H. Wu, J. Chen, W. Zhou, G. Wu, Z. Xiong, T. Zhang and P. Chen, *Phys. Chem. Chem. Phys.*, 2013, **15**, 10487-10493.
43. K. Kohata, T. Fukuyama and K. Kuchitsu, *J. Phys. Chem.*, 1982, **86**, 602-606.
44. M. R. Hartman, J. J. Rush, T. J. Udovic, R. C. Bowman Jr and S.-J. Hwang, *J. Solid State Chem.*, 2007, **180**, 1298-1305.
45. W. T. Klooster, T. F. Koetzle, P. E. M. Siegbahn, T. B. Richardson and R. H. Crabtree, *J. Am. Chem. Soc.*, 1999, **121**, 6337-6343.
46. J. P. Contour and G. Pannetier, *J. Catal.*, 1972, **24**, 434-445.
47. X. Chen, T. Zhang, P. Ying, M. Zheng, W. Wu, L. Xia, T. Li, X. Wang and C. Li, *Chem. Commun.*, 2002, 288-289.
48. L. Ding, Y. Shu, A. Wang, M. Zheng, L. Li, X. Wang and T. Zhang, *Appl. Catal., A*, 2010, **385**, 232-237.
49. X. Zheng, G. Wu, W. Li, Z. Xiong, T. He, J. Guo, H. Chen and P. Chen, *Energy Environ. Sci.*, 2011, **4**, 3593-3600.
50. D. J. Heldebrant, A. Karkamkar, N. J. Hess, M. Bowden, S. Rassat, F. Zheng, K. Rappe and T. Autrey, *Chem. Mater.*, 2008, **20**, 5332-5336.
51. Y. S. Chua, P. Chen, G. Wu and Z. Xiong, *Chem. Commun.*, 2011, **47**, 5116-5129.
52. F. H. Stephens, V. Pons and R. T. Baker, *J. Chem. Soc., Dalton Trans.*, 2007, 2613-2626.
53. M. Szwarc, *Proc. R. Soc. London, Ser. A*, 1949, **198**, 267-284.
54. I. P. Fisher and G. A. Heath, *Nature*, 1965, **208**, 1199-1200.
55. D. Y. Kim, N. J. Singh, H. M. Lee and K. S. Kim, *Chem. Eur. J.*, 2009, **15**, 5598-5604.
56. T. B. Lee and M. L. McKee, *Inorg. Chem.*, 2009, **48**, 7564-7575.
57. A. T. Luedtke and T. Autrey, *Inorg. Chem.*, 2010, **49**, 3905-3910.